HHS Public Access

Author manuscript

J Immunol. Author manuscript; available in PMC 2018 January 01.

Published in final edited form as:

J Immunol. 2017 January 01; 198(1): 492–504. doi:10.4049/jimmunol.1501845.

Essential Role of mTORC1 in Self-renewal of Murine Alveolar Macrophages

Wenhai Deng[*,†], **Jialong Yang**[†], **Xingguang Lin**[*], **Jinwook Shin**[†], **Jimin Gao**[*], and **Xiao-Ping Zhong**[†,‡,§,¶]

[*]School of Laboratory Medicine, Wenzhou Medical University, Wenzhou, Zhejiang 325035, China

[†]Department of Pediatrics, Division of Allergy and Immunology, Duke University Medical Center, Durham, NC 27710, USA

[‡]Department of Immunology, Duke University Medical Center, Durham, NC 27710, USA

[§]Hematologic Malignancies and Cellular Therapies Program, Duke Cancer Institute, Duke University Medical Center, Durham, NC 27710, USA

Abstract

Alveolar macrophages (AMΦ) have the capacity of local self-renewal through adult life; however, mechanisms that regulate AMΦ self-renewal remain poorly understood. We found that myeloid specific deletion of Raptor, an essential component of the mammalian/mechanistic target of rapamycin complex 1 (mTORC1), resulted in a marked decrease of this population of cells accompanying altered phenotypic features and impaired phagocytosis activity. We demonstrated further that Raptor/mTORC1 deficiency did not affect AMΦ development, but compromised its proliferative activity at cell cycle entry in the steady state as well as in the context of repopulation in irradiation chimeras. Mechanically, mTORC1 confers AMΦ optimal responsiveness to GM-CSF induced proliferation. Thus, our results demonstrate an essential role of mTORC1 for AMΦ homeostasis by regulating proliferative renewal.

Keywords

Alveolar Macrophage; mTOR; GM-CSF; Proliferation; Phagocytosis

Introduction

Alveolar macrophages (AMΦ) are the most abundant immune cells residing in terminal airways, where they play important functions in lung development, integrity, surfactant metabolism, and host defense responses, rendering them prominent targets for therapeutic intervention (1, 2). The traditional view that AMΦ belong to the mononuclear phagocyte

[¶]Correspondence Author: Xiao-Ping Zhong, MD, PhD, Department of Pediatrics-Division of Allergy and Immunology, Duke University Medical Center, Box 2644, Durham, NC 27710, Phone: 919-681-9450, Fax: 919-668-3750, xiaoping.zhong@duke.edu; Jimin Gao, MD, PhD, Zhejiang Provincial Key Lab for Technology and Application of Model Organisms, Wenzhou Medical University, Wenzhou, Zhejiang 325035, China. jimingao@yahoo.com.

Author contributions: WD designed and performed experiments, analyzed data, and wrote the paper. JY, XL, and JS performed experiments. JG participated in data analysis. XPZ designed experiments, participated in data analysis, and wrote the paper.

system (3) with bone marrow-derived monocytes as developmental intermediates has been recently challenged. Accumulating evidence has recently indicated that many tissue resident macrophages, including AMΦ, are derived from embryonic precursors, and are self-maintained with minimal contribution from circulating bone marrow-derived precursors in steady states (4–10). Fetal monocytes, as AMΦ precursors, seed into the lung prior to birth, expand massively, and then develop into mature AMΦ during the first week after birth. These differentiated AMΦ persist through adulthood via proliferative self-renewal independent of circulating monocytes (11). However, under certain conditions, such as bone marrow transplantation after lethal irradiation, AMΦ can be replenished from bone marrow-derived monocytes (8, 12, 13), which serves as an emergency pathway of AMΦ ontogeny. During AMΦ development, they undergo profound changes of the surface profile, which are characterized by increased expression of CD11c, Siglec-F, F4/80, and CD64, and concomitantly down-regulation of CD11b (11, 13). Local environmental signals, such as granulocyte-macrophage colony-stimulating factor (GM-CSF), instruct AMΦ via PPAR-γ to acquire such signature phenotypes and functions (13–15). Moreover, GM-CSF is also required for AMΦ maintenance in promoting proliferation (8, 16–19). Although emerging evidence highlights proliferative self-renewal as the main mechanism for AMΦ maintenance in both steady state and under stress conditions, mechanisms that link mitogenic stimuli, such as GM-CSF, to proliferative renewal programming, remain largely unknown.

Proliferating animal cells must tightly coordinate cell-cycle progression with cell growth and proliferation associated bioenergetic demand. Mechanistic target of rapamycin (mTOR), a highly conserved serine-threonine kinase, serves a key sensor for metabolic cues to regulate cell growth and proliferation (20, 21). mTOR forms at least two known distinct complexes, mTOR complex 1 (mTORC1) and mTORC2. mTORC1 contains mTOR, Deptor, mLST8, PRAS40 and the adapter protein Raptor, and is sensitive to the immunosuppressant rapamycin. mTORC1 acts downstream of the PI(3)K-Akt-Tsc1/2 pathway to phosphorylate translational regulators, the S6 ribosomal kinase (S6K), and the translation initiation factor 4E binding protein 1 (4E-BP1) (22). Subsequently, S6K phosphorylates the ribosomal protein S6 to promote ribosomogenesis. Furthermore, activation of mTORC1 promotes the downstream anabolic processes, such as glycolysis, by activating the transcriptional factors Hif1α and c-Myc, as well as *de novo* lipid biosynthesis via up-regulating SREBPs, while suppressing catabolic processes such as autophagy (20, 21, 23, 24). As such, essential roles of mTORC1 and its tight regulation by Tsc1 have been demonstrated to regulate both innate and adaptive immunity (25–40). While inhibition of mTORC1 can reduce pro-inflammatory cytokine production and M1 polarization by macrophages, constitutive mTORC1 activation due to Tsc1 deletion leads to enhanced pro-inflammatory responses and macrophage M1 polarization, but resistance to IL-4-induced M2 polarization and endotoxin-tolerance (41–44). Despite extensive progress in our understanding of the role of mTORC1 in macrophage function, the importance of mTORC1 signaling in the development or maintenance of macrophages is largely unclear. In this report, we demonstrated an essential role of mTORC1 in AMΦ homeostasis, at least in part by promoting their proliferative self-renewal via ensuring optimal responsiveness to GM-CSF induced cell cycle entry.

Materials and Methods

Mice

Rptor$^{fl/fl}$, *LyzM*$^{cre/+}$, *R26*$^{Zsgreen/+}$ (containing the robust bright reporter gene *Zsgreen* following the *STOP* cassette driven by the endogenous Rosa26 promoter) mice were purchased from Jackson Laboratory. *Rptor*$^{fl/fl}$ mice were crossed with *LyzM*$^{cre/+}$ mice or *R26*$^{CreERT2/+}$ to generate *Rptor*$^{fl/fl}$*LyzM*$^{cre/+}$ (called Rptor$^{\Delta Myel}$ here) or *Rptor*$^{fl/fl}$*R26*$^{CreERT2/+}$ mice, respectively. To monitor the activity of Cre recombinase, *LyzM*$^{cre/+}$ and *Rptor*$^{\Delta Myel}$ mice were further mated with *R26*$^{Zsgreen/+}$ mice. All mice were in *C57BL/6* genetic background. Experiments were carried on 6–9 week old mice unless otherwise indicated. All procedures were in compliance with protocols approved by the IACUC of Duke University.

Cell isolation

Bronchoalveolar lavage was performed by repeatedly passing 0.5ml cold PBS with 2mM EDTA through an intratracheal cannula (BD Insyte IV catheter) 5 times. Peritoneal cells were collected by lavage with 5ml cold PBS with 2mM EDTA. Bone marrow cells were harvested by flushing tibias and femurs. Splenocytes were obtained by mechanical dissociation of spleen tissues. To isolate cells from the lung, whole lungs were cut into small pieces, and digested in RPMI-1640 medium supplemented with 2% fetal bovine serum (FBS), 2mg/ml type IV Collagenase (Washington), and 0.05mg/ml DNase I(Sigma-Aldrich) for 45 min at 37°C. Red blood cells were lysed in ACK buffer for 3 min on ice. All cells were filtered through nylon meshes and washed with cold PBS.

Cell stimulation and culture

Fleshly isolated cells were rested in PBS supplemented with 0.5–1% FBS for 2h. Then, they were stimulated with varying doses of recombinant murine GM-CSF (Peprotech), recombinant murine M-CSF (Peprotech) or vehicle (PBS) for 30 min. In some experiments, cells were pretreated by rapamycin (Sigma-Aldrich) as indicated. For an *in vitro* culture assay, cells harvested by bronchoalveolar lavage were labeled with CFSE or CellTrace where indicated. Cells were cultured in complete RPMI-1640 medium containing 10% FBS, 2 mM glutamine, and penicillin and streptomycin (100 U/ml each; Invitrogen) for 1–2 h at 37°C and 5% CO_2. The non-adherent cells were discarded, and the plates were washed by warm PBS twice. The remaining adherent cells were used as alveolar macrophages, and were cultured in the presence of 10 ng/ML LPS (Sigma-Aldrich), 10 ng/ML recombinant murine IL-4 (Peprotech), 10 ng/ML recombinant murine GM-CSF, recombinant murine M-CSF or vehicle (PBS) for the indicated times. The cultured cells constituted more than 95% as alveolar macrophages verified by flow cytometry analysis. GlogiPlug (BD Bioscience) was added if intracellular flow cytometry analysis required. 0.5 μM 4-OHT (4-hydroxy-tamoxifen; Sigma-Aldrich) were administered into the culture medium for the induction of Cre-mediated deletion.

Flow cytometry

For analysis of surface markers, cells were stained for 15 min on ice in PBS supplemented with 2% FBS with antibodies from Biolegend, unless specified otherwise. These antibodies were FITC, PE, PerCP, PE-Cy7, APC/Alexa Fluor 647, or APC-Cy7 conjugated anti-CD115 (AFS98), anti-CD116 (698423; R&D), anti-CD131 (JORO50; BD), anti-Siglec-F (E50-2440; BD), anti-CD11c (N418), anti-CD11b (M1/70), anti-CD45.1 (A20), anti-CD45.2 (104), anti-I-A/I-E (M5/114.15.2), anti-F4/80 (BM8), anti-Ly6C (HK1.4), anti-CD98 (RL388), anti-CD80 (16-10A1), anti-CD86 (GL-1), anti-CD16/32 (93), anti-CD64 (X54-5/7.1), anti-CD205 (NLDC-145), anti-CD206 (C068C2), anti-CD3 (145-2C11), anti-TCR-β (H57-597), anti-NK1.1 (PK136), anti-CD19 (6D5), anti-B220 (RA3-6B2), anti-Ly6G (1A8), and anti-CD103 (2E7). CD115, CD116, and CD131 were stained for 30 min at room temperature. A Pacific blue conjugated live/dead viability kit or 7-AAD (Invitrogen) was used for the exclusion of dead cells. For assessment of apoptosis, Annexin-V and FITC-VAD-FMK (Promega) staining kits were applied.

For detection of intracellular cytokine or phosphorylated signaling proteins, fleshly isolated cells or stimulated cells were fixed using BD cyto/perm buffer according to manufacturer's instructions. Following permeabilization with pre-chilled pure methanol (−20°C) for at least 30 min on ice, intracellular staining was performed with antibodies, including anti-IL-12 (p40) –PE (C15.6; Biolegend), anti-pS6 (Ser235/236)-Alexa Fluor 647 (D57.2.2E; Cell signaling) and anti-p4E-BP1 (Thr37/46; 236B4; Cell Signaling). Anti-p4E-BP1 was detected with anti-rabbit-IgG-Alexa Fluor 594 (Invitrogen). Isotype-matched control antibodies were used as a negative control.

We noted that *Raptor* deficiency AMΦ exhibited elevated autofluorescence compared with WT controls (Figure 2A, Supplementary Figure S2A). As a source of noise, autofluorescence may decrease sensitivity to distinguish the levels of individual antigen markers (65). To unequivocally determine the surface phenotypes of AMΦ, we adapted fluorescence-minus-one (FMO) staining sets in which a channel of interest was stained with isotype antibodies to establish autofluorescence control, and the expression of each marker was quantified by dividing the geometric mean fluorescence intensity (gMFI) of the molecule of interest of the stained cells by the gMFI of FMO control. Data were acquired on BD Canto II and analyzed with Flowjo software (Tree Star).

Cell sorting and quantitative real-time PCR

Cells isolated from whole lungs were stained with PE conjugated antibody against Siglec-F, followed by enrichment by MACS (Miltenyi biotec) positive selection with LS columns according to the manufacture's protocol. The enriched cells were stained with anti-CD11c and 7-AAD. Live alveolar macrophages were sorted using MoFlo with greater than 98% purity. Total RNA was extracted by the TRIZOL method, and then reversely transcribed to cDNA using an iScript kit (Bio-Rad). qPCR was performed with SYBR Green master mix (Bioline) on a Mastercycler realplex system (Eppendorf). Relative expression of each gene was measured using the delta Ct method, and the expression of beta actin served as a standard (Primers were listed in the supplementary table 1). Each PCR reaction was verified by a melting curve or agarose gel electrophoresis.

Apoptotic phagocytosis assay

Phagocytosis of apoptotic cells was conducted as previously described. Briefly, thymocytes were cultured with 0.1 μM dexamethasone (Alfa Aesar) for 16 h to induce apoptosis. After pHrodo Red (Invitrogen) labeling, apoptotic thymocytes were incubated with purified alveolar macrophages in 12-well plates. Alveolar macrophages were scraped off from the plate and analyzed by flow cytometry.

Assessment of proliferation

Proliferation was assessed by analysis of BrdU (Sigma-Aldrich) incorporation cells in vitro and in vivo following incubation of 10 uM BrdU in culture medium for 6–8 h or injection i.p. with 1.5 mg BrdU in 200 ul PBS for 7 consecutive days, respectively. The harvested cells were stained for surface markers, followed by intracellular staining for the BrdU according to the manufacture's introduction (BD Biosciences). Frequencies of BrdU incorporation were determined by flow cytometry using corresponding cells stained by an isotype antibody as background controls. Ki67 expression was determined by intracellular staining and flow cytometry.

Measurement of glucose uptake

Glucose uptake was measured with 2-NBDG (2-(N-(7-Nitrobenz-2-oxa-1,3-diazol-4-yl)Amino)-2-Deoxyglucose; Invitrogen). Freshly isolated cells were incubated with 100 μM 2-NBDG for 10 min at 37°C prior to the staining of surface markers.

Analysis of mitochondrial mass

For mitochondrial mass, cells were stained with 50 nM MitoTracker Green (Invitrogen) in complete medium at 37°C for 30 min prior to surface staining. Alternatively, relative mitochondrial genomic DNA copies were determined by isolating total DNA from sorted cells and performing real-time quantitative PCR using the mitochondrial 12S rRNA and nuclear 18S rRNA specific primers as previously described(39).

Mixed bone marrow chimeras

The recipient mice ($CD45.1^+CD45.2^+$) were exposed to lethal irradiation (1000 rad). The mixture of T cells depleted bone marrow cells from wild-type mice($CD45.1^+$) and $Rptor^{\Delta Myel}$ mice($CD45.2^+$), or wild-type mice ($CD45.1^+$) and $Rptor^{fl/fl}R26^{CreERT2/+}$ ($CD45.2^+$) were injected i.v. into the recipient mice at indicated ratio, respectively. Eight weeks later, recipient mice were sacrificed at various time points, depending on the requirements of the experiments. For the induction of the Cre recombination by tamoxifen, 200 μl 10mg/μl tamoxifen (Sigma-Aldrich) were injected i.p. into the recipient mice at least 4 times before analysis.

Statistical analysis

Data were calculated with the mean SEM method. Unless specified differently, statistics were determined using unpaired two-tailed Student's *t* test using Prism software (GraphPad).

Results

Myeloid specific Raptor deficiency leads to selective disruption of AMΦ homeostasis

To investigate the role of mTORC1 in resident macrophages, we generated mice that were homozygous for the floxed *Raptor* gene, a key component of the mTORC1 complex (20), and heterozygous for the *Cre* recombinase gene driven by the lysozyme M promoter (45) (referred as $Rptor^{\Delta myel}$). Littermates bearing the floxed *Raptor* gene in the absence of *Cre* served as wild-type controls (referred as WT). In $Rptor^{\Delta myel}$ mice ranging from 6 to 16 weeks of age, AMΦ ($CD11c^{+}Siglec\text{-}F^{+}$) were obviously decreased in both frequencies and absolute numbers compared to WT controls (Figure 1A, 1B). Evaluation of additional cell surface markers for AMΦ further confirmed the reduction of this population of cells in $Rptor^{\Delta myel}$ mice (Supplementary Figure S1A). Since fetal monocytes, which serve as AMΦ precursors, seed the lung before birth and initially establish the AMΦ pool in the first week after birth(11), we asked whether impaired AMΦ development in the absence of *Raptor* contributed to decreased AMΦ in adult mice. However, no obvious differences in either frequencies or numbers of AMΦ were observed between $Rptor^{\Delta myel}$ and WT mice at 7 days of age (Figure 1C and 1D). Accordingly, mRNA expression of *PU.1* and *PPAR-γ*, which were critical for AMΦ differentiation (13, 46), were comparable between sorted AMΦ from WT and $Rptor^{\Delta Myel}$ mice (Figure 1E). These findings suggest that loss of mTORC1 did not impair initial establishment of the AMΦ pool; rather, it caused impaired maintenance or further expansion of this population of cells.

To determine whether mTORC1 plays a broad role in macrophage generation and maintenance, we analyzed macrophages from various tissues. Different from AMΦ, total numbers of other tissue macrophages such as large peritoneal macrophages (LPΦ), small peritoneal macrophages (SPΦ), splenic red-pulp macrophages (RPΦ) and bone marrow macrophages (BMΦ) were not obviously affected in $Rptor^{\Delta myel}$ mice. Moreover, there were no changes in the pool size of interstitial macrophages (IMΦ) as the counterparts of AMΦ located in the lung, which indicated normal development or recruitment of these macrophages in the absence of *Raptor* (Figure 1F and supplementary Figure S1B).

To rule out the possibility that differential *Cre*-mediated deletion efficiencies in these cell lead to such distinct phenotypes between AMΦ at the age of adult and 7 days after birth, as well as other macrophages, we bred $Rptor^{\Delta myel}$ mice to $R26^{Zsgreen/+}$ reporter mice which carrying a floxed STOP cassette preceding the robust bright fluorescent protein *Zsgreen* gene in the ubiquitously active Rosa26 locus (47). We observed similarly high efficient *Cre*-mediated deletion in AMΦ (Figure 1G), even at 7 days of age (Figure 1H), and other macrophages in both $LyzM^{Cre/+}R26^{Zsgreen/+}$ and $Rptor^{\Delta myel}R26^{Zsgreen/+}$ mice (Figure 1I). Furthermore, no significant alterations were observed in the numbers of other hematopoietic cells in the lung (Figure 1J), neither in peripheral blood cells (not depicted). Collectively, Raptor/mTORC1 was selectively required for AMΦ homeostasis and had minimal role in the maintenance of other macrophages.

Rptor$^{\Delta myel}$ AMΦ exhibit abnormal surface phenotype, M1/M2 polarization, and phagocytosis function

AMΦ exhibit phenotypic characteristics including high autofluorescence featured by broad excitation and emission wavelengths (Supplementary Figure S2A), highly expressed Siglec-F and CD11c, and yet low expression of CD11b, which may reflect the local specific signals these cells received (1, 2). Rptor$^{\Delta Myel}$ AMΦ displayed enhanced autofluorescence (Figure 2A and Supplementary Figure S2A), down regulated Siglec-F, but elevated CD11c and CD11b expression compared with WT controls (Figure 2B, C), correlated with altered mRNA expression (Figure 2D). Furthermore, surface expression of pan-macrophage markers F4/80 and CD64 were decreased on AMΦ from Rptor$^{\Delta Myel}$ mice (Figure 2E). Analysis of the expression of other surfaces markers, such as MHC-II and co-stimulatory molecules CD80 and CD86, revealed down regulation of these molecules to different extents (Figure 2E). Overall, these findings indicated that deletion of *Raptor* broadly affected phenotypic characteristics of AMΦ.

Dysregulation of AMΦ in adult Rptor$^{\Delta Myel}$ mice was in a manner reminiscent of those in immature AMΦ in terms of the outcome of arrested developmental process (11, 13, 48). It raised the possibility that fetal monocytes may be defective to develop into *bona fide* mature AMΦ in the absence of Raptor. However, AMΦ from Rptor$^{\Delta myel}$ mice at the age of postnatal day 7 showed similar autofluorescence (Figure 2A) and similar expression of Siglec-F, CD11b, and CD11c relative to the WT AMΦ (Figure 2F), arguing against the possibility of impaired development of mature AMΦ in Rptor$^{\Delta myel}$ mice. Thus, it was more likely that functional mTORC1 had a direct or indirect function in maintaining the characteristic surface profile of AMΦ. Together with the unaltered initial AMΦ population established in the first week after birth, our data suggested that *Raptor* deficiency may not affect AMΦ development, but may result in diminished AMΦ with altered surface profile over time.

Rptor$^{\Delta myel}$ AMΦ exhibit abnormal M1/M2 polarization and phagocytosis function

Macrophages can differentiation to M1 and M2 subleanages with distinct functions []. Rptor$^{\Delta myel}$ AMΦ appeared to manifest enhanced inflammatory responses, reflected by elevated IL-12 and iNOS expression following LPS stimulation, but to be refractory to IL-4-induced M2 polarization indicated by decreased expression of the M2 hallmark gene *Chi3l3(YM1)* (Figures 3A and 3B). Additionally, Rptor$^{\Delta myel}$ AMΦ expressed slightly reduced CD206, another M2 marker (Figure 2E). Together, our data suggest that absence of mTORC1 activity promotes M1 but inhibits M2 polarization of AMΦ.

AMΦ contribute to lung tissue homeostasis by clearing up dying cells from the bronchoalveolar space. To characterize the capacity of AMΦ from WT and Rptor$^{\Delta myel}$ mice to phagocytose apoptotic cells, we took advantage of pHrodo Red, a dye that only fluoresces following transport into acidic environments, such as lysosomes(49). Purified AMΦ from WT and Rptor$^{\Delta myel}$ mice were incubated with pHrodo Red-labeled apoptotic thymocytes *in vitro* for the indicated times, followed by flow cytometric detection of pHrode Red. pHrode Red fluorescence was consistently lower in Rptor$^{\Delta myel}$ AMΦ than WT controls (Figures 3C and 3D), indicating impaired capacity of Rptor$^{\Delta myel}$ AMΦ to engulf apoptotic cells.

mTORC1 dependent metabolic checkpoint mediates AMΦ proliferation

Since AMΦ are generally restricted to the alveoli(50, 51) and have recently been demonstrated to persist through adulthood with long lifespan and local proliferation independently of circulating monocytes(8, 11), we hypothesized that the diminished density of AMΦ in the absence of Raptor could be due to defect in viability, proliferation, or both. We detected similar proportions of dead cells identified by 7-AAD or Annexin-V staining (Supplementary Figure S3A), and similar caspase activity by VAD-FMK staining (Supplementary Figure S3B) in AMΦ from WT and Rptor$^{\Delta Myel}$ mice, suggesting that mTORC1 may be dispensable for AMΦ survival.

AMΦ have the capacity of self-renewal *in situ* at a slow rate[1]. Indeed, BrdU labeling assay revealed ~20% of WT AMΦ entered the cell-cycle after consecutive 7 d BrdU administration, whereas other hematopoietic cells like monocytes constituted more than 90% of cells incorporated with BrdU (Figure 4A and 4B). In comparison, Rptor$^{\Delta Myel}$ AMΦ showed around half of the population entered the cell-cycle relative to WT AMΦ (Figure 4A and 4B). Expression of Ki67, which is expressed exclusively by cells in active cycling, was also decreased in Rptor$^{\Delta Myel}$ AMΦ (Figure 4C). In contrast to AMΦ, no obvious differences in BrdU incorporation were observed in other monocyte/macrophage lineage cells, such as IMΦ, RPΦ, and monocytes (Figure 4B), which were in agreement with normal cellularity of these cells (Figure 1F).

Consistent with impaired proliferation, Rptor$^{\Delta Myel}$ AMΦ showed diminished expression of *CDK2*, *CDK4*, *CDK6,* and *Cyclin D2* (*CCND2*), components of the cell cycle machinery (Figure 4D). Thus, defective in cell-cycle entry of Rptor$^{\Delta Myel}$ AMΦ may potentially contribute to impaired self-renewal and diminished AMΦ population in these mice.

Next, we sought to determine the cellular mechanism correlated with mTORC1 that regulates the proliferation of AMΦ. We noted that Rptor$^{\Delta Myel}$ AMΦ showed a significantly reduced cell size, as judged by the flow cytometry forward scatter (Figure 4E). Proceedings of cell growth and proliferation generally coincide with the enhanced uptake of nutrients, such as amino acids and glucose. Expression of CD98, a key molecule for the amino acid uptake, and glucose uptake were both down regulated in Rptor$^{\Delta Myel}$ AMΦ (Figure 4F). Mitochondrial contents in Rptor$^{\Delta Myel}$ AMΦ were also reduced, indicated by decreased MitroTracker staining (Figure 4G and 4H) and the mitochondrial DNA to nuclear DNA ratio (Figure 4I). These data suggested an essential role of *Raptor* for AMΦ growth, nutrient uptake, and mitochondria biosynthesis, which may contribute to cell-cycle entry and self-renewal of AMΦ.

Raptor regulates repopulation of AMΦ post irradiation induced replenishment

Studies have shown that most tissue macrophages, including AMΦ, can be replenished by bone marrow-derived blood monocytes in the context of irradiation chimeras (8, 11–13). We then asked whether *Raptor* is also required for proliferation of AMΦ originated from bone marrow-derived monocytes. For this purpose, we generated chimeras by adoptive transfer of

[1]Abreviations: mammalian/mechanistic target of rapamycin, mTOR; Alveolar macrophage, AMΦ; Large peritoneal macrophage, LPΦ.

a mixture of bone marrow cells from WT ($CD45.1^+$) and $Rptor^{\Delta myel}$ ($CD45.2^+$) mice at a 1:2 ratio into lethally irradiated WT hosts ($CD45.1^+CD45.2^+$). At 8 weeks after irradiation, analysis of monocytes in the peripheral blood, spleen, and lung of host mice indicated complete hematopoietic chimerism with WT and $Rptor^{\Delta myel}$ close to the input 1:2 ratio (Figure 5A). The WT to $Rptor^{\Delta myel}$ ratio of IMΦ in the host was also close to 1:2 (Figure 5A), accompanying about 2 folds more $Rptor^{\Delta myel}$ IMΦ than WT IMΦ in the host lung (Figure 5B). These data suggested that the recruitment and differentiation of blood-derived monocytes to IMΦ might not be obviously affected by mTORC1 deficiency. However, the ratio between donor-derived WT and *Raptor* deficient AMΦ was inverted to 2:1, accompanying obviously less $Rptor^{\Delta myel}$ AMΦ than WT AMΦ in the host lung (Figure 5B). These data indicated that *Raptor* deficient AMΦ were less efficient than *Raptor* sufficient cells in repopulating the AMΦ pool (Figure 5A). WT and *Raptor* deficient AMΦ exhibited similar levels of autofluorescence (data not depicted). However, AMΦ signature markers, with the exception of CD11c, were altered in the same pattern as in individual mice of the relevant genotype (Figure 5C). Furthermore, cell size (Figure 5D), CD98 expression, glucose uptake, and mitochondrial contents were all decreased (Figure 5E). Thus, Raptor/mTORC1 intrinsically regulates the phenotypic characteristics and metabolism in AMΦ.

The reduced AMΦ population from $Rptor^{\Delta myel}$ donors could be a result of defects in recruitment of the monocyte to the lung, in monocyte differentiation to AMΦ, or in AMΦ self-renewal after differentiation. To pinpoint the role of mTORC1 in AMΦ self-renewal, we generated mixed bone marrow chimeric mice using WT ($CD45.1^+$) and $Rptor^{fl/fl}R26^{CreERT2/+}$ ($CD45.2^+$) donor mice in lethally irradiated host mice ($CD45.1^+CD45.2^+$). Eight weeks after reconstitution, when the AMΦ pool had been essentially reestablished as previously reported (8, 12, 13), recipient mice were given tamoxifen daily for a total of 4 times to delete *Raptor*. The relative ratios of *Raptor* deficient AMΦ but not splenic B cells or IMΦ to their respective WT controls were progressively decreased in the chimeric mice 2 to 4 weeks after tamoxifen administration (Figure 5F), correlated with decreased $Ki67^+$ expression and cell size in *Raptor* deficient AMΦ (Figure 5G).

Together, these observations support that mTORC1 is important for self-renewal of AMΦ and for replenishing this pool of cells *in vivo*. The unhindered population of IMΦ in the absences of Raptor suggests that recruitment of monocytes to lung is absolutely dependent on mTORC1. However, we recognize that our data do not rule out that Raptor/mTORC1 may play a role for macrophages to migrate to the alveolar compartment of the lung.

mTOR1 signaling confers AMΦ optimal proliferating capacity in response to GM-CSF

A critical question remains to be addressed: which receptor(s) activate mTORC1 to ensure AMΦ self-renewal? A previous study identified both M-CSF and GM-CSF as tissue-derived signals that contribute to local proliferation of AMΦ(8). Indeed, we observed that AMΦ expressed CD115 (M-CSF receptor), as well as CD116 and CD131 (components of GM-CSF receptor) (Figure 6A). *In vitro*, GM-CSF induced robust division of CFSE-labeled WT AMΦ (Figure 6B). Although M-CSF could also induce AMΦ proliferation, its activity was much weaker than GM-CSF (Figure 6B). S6 phosphorylation, a hallmark event of mTORC1

activity, could be induced in AMΦ following GM-CSF treatment in a dose-dependent manner (Figure 6C). Contrarily, M-CSF failed to induce obvious S6 phosphorylation in AMΦ (Figure 6C), even though the same concentrations of M-CSF readily induced S6 phosphorylation in LPΦ (Figure 6D). GM-CSF-induced S6 phosphorylation could be inhibited by rapamycin (Figure 6E) and was ablated in Rptor$^{\Delta Myel}$ AMΦ (Figure 6F). Phosphorylation of 4E-BP1, another mTORC1 substrate, was also decreased in Rptor$^{\Delta Myel}$ AMΦ (Figure 6F). We also observed impairment of mTORC1 signaling in Rptor$^{\Delta Myel}$ AMΦ from 7 day old mice (Figure 6G). Together, these observations demonstrated that GM-CSF is a potent upstream mTORC1 activator in AMΦ.

To directly assess the effect of mTORC1 deficiency on GM-CSF induced AMΦ proliferation, we co-cultured equal numbers of CellTrace dye-labeled WT (*Zsgreen* reporter negative) and Rptor$^{\Delta Myel}$R26$^{Zsgreen/+}$ (*Zsgreen* reporter positive) AMΦ in the presence of GM-CSF *in vitro*. After 5 days of incubation, *Zsgreen*$^{+}$ Rptor$^{\Delta myel}$ AMΦ proliferated less than *Zsgreen*$^{-}$WT counterparts (Figure 7A), which correlated to 50% decrease of Rptor$^{\Delta Myel}$ AMΦ residing in the S-phase, revealed by BrdU incorporation (Figure 7B). Moreover, "acute" deletion of *Raptor* in AMΦ during *in vitro* culture confirmed the importance of mTORC1 signaling for AMΦ optimal proliferative responsiveness to GM-CSF stimulation (Figure 7C – 7E). These observations, with those shown in Figure 4A – 4C, demonstrated that mTORC1 signaling is necessary for GM-CSF induced AMΦ expansion *in vitro* and *in vivo*.

GM-CSF efficiently induces metabolic reprogramming in AMΦ, seen in up-regulation of transcription factors *c-Myc* and *Hif1a,* which are important players in glycolysis and cell-cycle entry, as well as the molecules involved in glycolytic activity (*Hk2, Ldha*, and *Tpi1*), and *de novo* lipid biosynthesis (*SREBP1* and *SREBP2*; Figure 7F). Strikingly, these metabolic responses to GM-CSF were markedly attenuated in Rptor$^{\Delta Myel}$ AMΦ.

Collectively, mTORC1 is required for AMΦ to respond optimally to GM-CSF to trigger proliferation and control metabolic reprogramming, such as glycolysis and lipid biosynthesis, to meet the energy demand for proliferation.

Discussion

Much emphasis has been placed on the identification of the embryonic origin of AMΦ with the capacity of self-renewal over the past few years (1, 2). In contrast, the underlying molecular events that mediate proliferative renewal for homeostatic maintenance of AMΦ are poorly defined, though the proliferative capacity of AMΦ was noted 40 years ago (52). Moreover, despite emerging evidence for GM-CSF to instruct the ontology and phenotype of AMΦ (11, 13–16, 48, 53), little is known about whether and how this tissue niche derived signal programs AMΦ self-renewal. Here, we demonstrate that mTORC1 signaling is essential for AMΦ self-renewal and that mTORC1 exerts its function at least in part by ensuring optimal responsiveness of AMΦ to GM-CSF induced cell cycle entry. Myeloid specific loss of Raptor/mTORC1 in mice results in selective reduction of AMΦ numbers correlated with defective proliferative capacity of these cells. Our study to the best of our

knowledge, therefore represents the first evidence that mTORC1 signaling is one of the main molecular events that orchestrates AMΦ self-renewal.

The gene expression heterogeneity among macrophages and marked diversity of anatomic locations in which these cells reside suggest that certain molecular events may affect the maintenance of specific macrophage populations. Indeed, Spi-C is especially required for the maintenance of iron-recycling macrophage residing in the spleen and bone marrow (54, 55), while studies using mice deficient in Gata6 revealed its selective role for the maintenance of the LPΦ population by regulating, proliferation, survival, and tissue localization (56–58). Our results uncover a novel tissue selective role for mTORC1 in the maintenance of AMΦ. It thus seems that the maintenance of other macrophages might be capable of bypassing mTORC1 signaling, or be compensated by other pathways converged at the level of the phosphorylation of S6, such as mitogen-activated protein kinases MEK/ERK pathways (59, 60).

Establishment and maintenance of the AMΦ population requires the initial population and differentiation of these cells from fetal monocytes (11, 13) and their subsequent proliferation and survival. Our data suggest that mTORC1 is not required for differentiation and initial population of AMΦ in the lung. On day 7 after birth, AMϕ are normal in both numbers, and in the expression of signature transcription factors such as *PU.1* and *PPAR-γ* (13, 46) for their development in $Rptor^{\Delta myel}$ mice. Although a recent study proposed that the widely used $LyzM^{cre/+}$ mice may not efficiently delete the gene of interest during the development of AMΦ(13), we readily detected essential expression of the reporter protein as indicator of *Cre* recombinase activities, and efficient abrogation of mTORC1 signaling in AMΦ in a uniform manner in $Rptor^{\Delta myel}$ mice, ruling out the possibility that unhindered development and population of AMϕ in early life is caused by inefficient deletion of *Raptor* in these mice. In contrast to minimal influence on AMΦ in early life, our data reveal that *Raptor* plays an important role in AMΦ proliferative self-renewal. We have found diminished dividing AMΦ in $Rptor^{\Delta myel}$ mice, marked by compromised cell-cycle entry and metabolic activities. Moreover, $Rptor^{\Delta myel}$ AMΦ display altered surface profiles and defective phagocytotic capacity, indicating that mTORC1 deficiency results in not only impaired proliferative renewal, but also loss of maturation integrity of AMΦ. The importance of mTORC1 for AMΦ proliferative renewal is further supported by our findings in a mixed bone marrow chimeras experiment, in which deletion of mTORC1 in established AMΦ leads to impaired AMΦ proliferative capacity for the homeostatic maintenance. Impaired viability of AMΦ has been noted upon the exposure to the mTOR inhibitor temsirolimus in vitro (59). However, we did not observe obvious survival defects in $Rptor^{\Delta myel}$ AMΦ. The difference is likely caused by a potential inhibition effect of mTORC2 by temsirolimus, which may affect Akt activation. Additionally, mTOR-independent functions of Raptor have recently revealed (61).

The heterogeneity of resident macrophages in different tissues implies that distinct tissue niche specific signals regulate local macrophage identities and homeostasis (15, 62). For example, omentum in the peritoneal cavity derived retinoic acid instructs the recruitment of LPΦ (58), while concomitant blockage of local GM-CSF and M-CSF compromised AMΦ repopulation after depletion(8). We sought to link the tissue signals that govern AMΦ

proliferation with mTORC1 signaling. Intriguingly, GM-CSF can induce mTORC1 activities in a dose-dependent manner, whereas the equivalent hematopoietic growth factor M-CSF fails to do so, even though the same concentrations of M-CSF readily induce mTORC1 activities in LPΦ. Consistently, GM-CSF show stronger capacity to promote AMΦ proliferation than M-CSF does. GM-CSF may induce AMΦ proliferation by promoting glycolysis and *de novo* lipogenesis through mTORC1 signaling. These essential bioenergetic pathways probably support the enhanced energetic demands associated with cellular proliferation. It would be of interest to determine how mTORC1 is activated downstream of GM-CSF receptor in AMΦ. Although we propose that mTORC1 may mediate GM-CSF signal to promote AMΦ self-renewal, our data do not rule out that other ligands/receptors may also regulate AMΦ self-renewal via mTORC1. GM-CSF has been found to signal via PU.1 and PPARγ in AMΦ (13, 46). However, PU.1 and PPARγ was not decreased in $Rptor^{\Delta myel}$ AMΦ, suggesting the possibility that GM-CSF may function through mTORC1 to promote AMF self-renewal apart from PU.1 and PPARγ. Further studies should determine if mTORC1 could participate in other signals presented in the local microenvironment to regulate AMΦ self-renewal.

Rapamycin has been used extensively for immunosuppression and anti-tumor therapies. Rapamycin induced pulmonary toxicity and interstitial pneumonitis have been reported with the underlying mechanisms remaining unclear (63). Previous studies showed impaired macrophage function in mice or from healthy human donors treated with rapamycin (64). Given the importance of mTORC1 for AMΦ homeostasis in mice, it is possible that inhibition of mTORC1 in human patients may similarly impair AMΦ homeostasis, which may consequently contribute to the pulmonary side effects of rapamycin in clinical settings.

In summary, our study has identified an essential role of mTORC1 for AMΦ maintenance, both in steady-state and during irradiation-induced repopulation. mTORC1 may mediate GM-CSF induced metabolic reprogramming for AMΦ proliferation. Our data provide a novel molecular basis that regulates proliferative renewal of resident macrophages in a selective tissue. Furthermore, the selective dependence of AMΦ homeostasis on mTORC1 signaling might provide potential targets for therapeutic intervention of pulmonary diseases mediated by AMΦ.

Supplementary Material

Refer to Web version on PubMed Central for supplementary material.

Acknowledgments

We thank Joyce Cheng for editing the manuscript and the Flow Cytometry Facility in Duke Cancer Institute for sorting service.

This study is supported by NIAID, NIH (R01AI079088 and R01AI101206).

References

1. Hussell T, Bell TJ. Alveolar macrophages: plasticity in a tissue-specific context. Nat Rev Immunol. 2014; 14:81–93. [PubMed: 24445666]

2. Kopf M, Schneider C, Nobs SP. The development and function of lung-resident macrophages and dendritic cells. Nat Immunol. 2015; 16:36–44. [PubMed: 25521683]

3. van Furth R, Cohn ZA, Hirsch JG, Humphrey JH, Spector WG, Langevoort HL. Mononuclear phagocytic system: new classification of macrophages, monocytes and of their cell line. Bullet World Health Organ. 1972; 47:651–658.

4. Ginhoux F, Greter M, Leboeuf M, Nandi S, See P, Gokhan S, Mehler MF, Conway SJ, Ng LG, Stanley ER, Samokhvalov IM, Merad M. Fate mapping analysis reveals that adult microglia derive from primitive macrophages. Science. 2010; 330:841–845. [PubMed: 20966214]

5. Schulz C, Gomez Perdiguero E, Chorro L, Szabo-Rogers H, Cagnard N, Kierdorf K, Prinz M, Wu B, Jacobsen SE, Pollard JW, Frampton J, Liu KJ, Geissmann F. A lineage of myeloid cells independent of Myb and hematopoietic stem cells. Science. 2012; 336:86–90. [PubMed: 22442384]

6. Hoeffel G, Wang Y, Greter M, See P, Teo P, Malleret B, Leboeuf M, Low D, Oller G, Almeida F, Choy SH, Grisotto M, Renia L, Conway SJ, Stanley ER, Chan JK, Ng LG, Samokhvalov IM, Merad M, Ginhoux F. Adult Langerhans cells derive predominantly from embryonic fetal liver monocytes with a minor contribution of yolk sac-derived macrophages. J Exp Med. 2012; 209:1167–1181. [PubMed: 22565823]

7. Yona S, Kim KW, Wolf Y, Mildner A, Varol D, Breker M, Strauss-Ayali D, Viukov S, Guilliams M, Misharin A, Hume DA, Perlman H, Malissen B, Zelzer E, Jung S. Fate mapping reveals origins and dynamics of monocytes and tissue macrophages under homeostasis. Immunity. 2013; 38:79–91. [PubMed: 23273845]

8. Hashimoto D, Chow A, Noizat C, Teo P, Beasley MB, Leboeuf M, Becker CD, See P, Price J, Lucas D, Greter M, Mortha A, Boyer SW, Forsberg EC, Tanaka M, van Rooijen N, Garcia-Sastre A, Stanley ER, Ginhoux F, Frenette PS, Merad M. Tissue-resident macrophages self-maintain locally throughout adult life with minimal contribution from circulating monocytes. Immunity. 2013; 38:792–804. [PubMed: 23601688]

9. Gomez Perdiguero E, Klapproth K, Schulz C, Busch K, Azzoni E, Crozet L, Garner H, Trouillet C, de Bruijn MF, Geissmann F, Rodewald HR. Tissue-resident macrophages originate from yolk-sac-derived erythro-myeloid progenitors. Nature. 2015; 518:547–551. [PubMed: 25470051]

10. Hoeffel G, Chen J, Lavin Y, Low D, Almeida FF, See P, Beaudin AE, Lum J, Low I, Forsberg EC, Poidinger M, Zolezzi F, Larbi A, Ng LG, Chan JK, Greter M, Becher B, Samokhvalov IM, Merad M, Ginhoux F. C-myb(+) erythro-myeloid progenitor-derived fetal monocytes give rise to adult tissue-resident macrophages. Immunity. 2015; 42:665–678. [PubMed: 25902481]

11. Guilliams M, De Kleer I, Henri S, Post S, Vanhoutte L, De Prijck S, Deswarte K, Malissen B, Hammad H, Lambrecht BN. Alveolar macrophages develop from fetal monocytes that differentiate into long-lived cells in the first week of life via GM-CSF. J Exp Med. 2013; 210:1977–1992. [PubMed: 24043763]

12. Landsman L, Jung S. Lung macrophages serve as obligatory intermediate between blood monocytes and alveolar macrophages. J Immunol. 2007; 179:3488–3494. [PubMed: 17785782]

13. Schneider C, Nobs SP, Kurrer M, Rehrauer H, Thiele C, Kopf M. Induction of the nuclear receptor PPAR-gamma by the cytokine GM-CSF is critical for the differentiation of fetal monocytes into alveolar macrophages. Nat Immunol. 2014; 15:1026–1037. [PubMed: 25263125]

14. Guth AM, Janssen WJ, Bosio CM, Crouch EC, Henson PM, Dow SW. Lung environment determines unique phenotype of alveolar macrophages. Am J Physiol Lung Cell Mol Physiol. 2009; 296:L936–946. [PubMed: 19304907]

15. Lavin Y, Winter D, Blecher-Gonen R, David E, Keren-Shaul H, Merad M, Jung S, Amit I. Tissue-resident macrophage enhancer landscapes are shaped by the local microenvironment. Cell. 2014; 159:1312–1326. [PubMed: 25480296]

16. Chen BD, Mueller M, Chou TH. Role of granulocyte/macrophage colony-stimulating factor in the regulation of murine alveolar macrophage proliferation and differentiation. J Immunol. 1988; 141:139–144. [PubMed: 3288696]

17. Higgins DM, Sanchez-Campillo J, Rosas-Taraco AG, Higgins JR, Lee EJ, Orme IM, Gonzalez-Juarrero M. Relative levels of M-CSF and GM-CSF influence the specific generation of macrophage populations during infection with Mycobacterium tuberculosis. J Immunol. 2008; 180:4892–4900. [PubMed: 18354213]

18. Nakata K, Akagawa KS, Fukayama M, Hayashi Y, Kadokura M, Tokunaga T. Granulocyte-macrophage colony-stimulating factor promotes the proliferation of human alveolar macrophages in vitro. J Immunol. 1991; 147:1266–1272. [PubMed: 1869822]
19. Fejer G, Wegner MD, Gyory I, Cohen I, Engelhard P, Voronov E, Manke T, Ruzsics Z, Dolken L, Prazeres da Costa O, Branzk N, Huber M, Prasse A, Schneider R, Apte RN, Galanos C, Freudenberg MA. Nontransformed, GM-CSF-dependent macrophage lines are a unique model to study tissue macrophage functions. Proc Natl Acad Sci U S A. 2013; 110:E2191–2198. [PubMed: 23708119]
20. Laplante M, Sabatini DM. mTOR signaling in growth control and disease. Cell. 2012; 149:274–293. [PubMed: 22500797]
21. Efeyan A, Comb WC, Sabatini DM. Nutrient-sensing mechanisms and pathways. Nature. 2015; 517:302–310. [PubMed: 25592535]
22. Duvel K, Yecies JL, Menon S, Raman P, Lipovsky AI, Souza AL, Triantafellow E, Ma Q, Gorski R, Cleaver S, Vander Heiden MG, MacKeigan JP, Finan PM, Clish CB, Murphy LO, Manning BD. Activation of a metabolic gene regulatory network downstream of mTOR complex 1. Mol Cell. 2010; 39:171–183. [PubMed: 20670887]
23. Lamming DW, Sabatini DM. A Central role for mTOR in lipid homeostasis. Cell Metab. 2013; 18:465–469. [PubMed: 23973332]
24. Dibble CC, Manning BD. Signal integration by mTORC1 coordinates nutrient input with biosynthetic output. Nat Cell Biol. 2013; 15:555–564. [PubMed: 23728461]
25. Wu Q, Liu Y, Chen C, Ikenoue T, Qiao Y, Li CS, Li W, Guan KL, Liu Y, Zheng P. The tuberous sclerosis complex-mammalian target of rapamycin pathway maintains the quiescence and survival of naive T cells. J Immunol. 2011; 187:1106–1112. [PubMed: 21709159]
26. Xie DL, Wu J, Lou YL, Zhong XP. Tumor suppressor TSC1 is critical for T-cell anergy. Proc Natl Acad Sci U S A. 2012; 109:14152–14157. [PubMed: 22891340]
27. Wu J, Shin J, Xie D, Wang H, Gao J, Zhong XP. Tuberous sclerosis 1 promotes invariant NKT cell anergy and inhibits invariant NKT cell-mediated antitumor immunity. J Immunol. 2014; 192:2643–2650. [PubMed: 24532578]
28. Yang K, Shrestha S, Zeng H, Karmaus PW, Neale G, Vogel P, Guertin DA, Lamb RF, Chi H. T cell exit from quiescence and differentiation into Th2 cells depend on Raptor-mTORC1-mediated metabolic reprogramming. Immunity. 2013; 39:1043–1056. [PubMed: 24315998]
29. Yang K, Neale G, Green DR, He W, Chi H. The tumor suppressor Tsc1 enforces quiescence of naive T cells to promote immune homeostasis and function. Nat Immunol. 2011; 12:888–897. [PubMed: 21765414]
30. Zeng H, Yang K, Cloer C, Neale G, Vogel P, Chi H. mTORC1 couples immune signals and metabolic programming to establish T(reg)-cell function. Nature. 2013; 499:485–490. [PubMed: 23812589]
31. Delgoffe GM, Kole TP, Zheng Y, Zarek PE, Matthews KL, Xiao B, Worley PF, Kozma SC, Powell JD. The mTOR kinase differentially regulates effector and regulatory T cell lineage commitment. Immunity. 2009; 30:832–844. [PubMed: 19538929]
32. Wang HX, Shin J, Wang S, Gorentla B, Lin X, Gao J, Qiu YR, Zhong XP. mTORC1 in Thymic Epithelial Cells Is Critical for Thymopoiesis, T-Cell Generation, and Temporal Control of gammadeltaT17 Development and TCRgamma/delta Recombination. PLoS Biol. 2016; 14:e1002370. [PubMed: 26889835]
33. Park Y, Jin HS, Lopez J, Elly C, Kim G, Murai M, Kronenberg M, Liu YC. TSC1 regulates the balance between effector and regulatory T cells. J Clin Invest. 2013; 123:5165–5178. [PubMed: 24270422]
34. Yang W, Gorentla B, Zhong XP, Shin J. mTOR and its tight regulation for iNKT cell development and effector function. Mol Immunol. 2015; 68:536–545. [PubMed: 26253278]
35. Shin J, Wang S, Deng W, Wu J, Gao J, Zhong XP. Mechanistic target of rapamycin complex 1 is critical for invariant natural killer T-cell development and effector function. Proc Natl Acad Sci U S A. 2014; 111:E776–783. [PubMed: 24516149]
36. Pan H, O'Brien TF, Wright G, Yang J, Shin J, Wright KL, Zhong XP. Critical role of the tumor suppressor tuberous sclerosis complex 1 in dendritic cell activation of CD4 T cells by promoting

MHC class II expression via IRF4 and CIITA. J Immunol. 2013; 191:699–707. [PubMed: 23776173]

37. Delgoffe GM, Pollizzi KN, Waickman AT, Heikamp E, Meyers DJ, Horton MR, Xiao B, Worley PF, Powell JD. The kinase mTOR regulates the differentiation of helper T cells through the selective activation of signaling by mTORC1 and mTORC2. Nat Immunol. 2011; 12:295–303. [PubMed: 21358638]
38. Shin J, Pan H, Zhong XP. Regulation of mast cell survival and function by tuberous sclerosis complex 1. Blood. 2012; 119:3306–3314. [PubMed: 22362037]
39. O'Brien TF, Gorentla BK, Xie D, Srivatsan S, McLeod IX, He YW, Zhong XP. Regulation of T-cell survival and mitochondrial homeostasis by TSC1. Eur J Immunol. 2011; 41:3361–3370. [PubMed: 21805467]
40. Lee K, Gudapati P, Dragovic S, Spencer C, Joyce S, Killeen N, Magnuson MA, Boothby M. Mammalian target of rapamycin protein complex 2 regulates differentiation of Th1 and Th2 cell subsets via distinct signaling pathways. Immunity. 2010; 32:743–753. [PubMed: 20620941]
41. Byles V, Covarrubias AJ, Ben-Sahra I, Lamming DW, Sabatini DM, Manning BD, Horng T. The TSC-mTOR pathway regulates macrophage polarization. Nat Commun. 2013; 4:2834. [PubMed: 24280772]
42. Zhu L, Yang T, Li L, Sun L, Hou Y, Hu X, Zhang L, Tian H, Zhao Q, Peng J, Zhang H, Wang R, Yang Z, Zhang L, Zhao Y. TSC1 controls macrophage polarization to prevent inflammatory disease. Nat Commun. 2014; 5:4696. [PubMed: 25175012]
43. Pan H, O'Brien TF, Zhang P, Zhong XP. The role of tuberous sclerosis complex 1 in regulating innate immunity. J Immunol. 2012; 188:3658–3666. [PubMed: 22412198]
44. Xie L, Sun F, Wang J, Mao X, Xie L, Yang SH, Su DM, Simpkins JW, Greenberg DA, Jin K. mTOR signaling inhibition modulates macrophage/microglia-mediated neuroinflammation and secondary injury via regulatory T cells after focal ischemia. J Immunol. 2014; 192:6009–6019. [PubMed: 24829408]
45. Clausen BE, Burkhardt C, Reith W, Renkawitz R, Forster I. Conditional gene targeting in macrophages and granulocytes using LysMcre mice. Transgenic Res. 1999; 8:265–277. [PubMed: 10621974]
46. Shibata Y, Berclaz PY, Chroneos ZC, Yoshida M, Whitsett JA, Trapnell BC. GM-CSF regulates alveolar macrophage differentiation and innate immunity in the lung through PU.1. Immunity. 2001; 15:557–567. [PubMed: 11672538]
47. Madisen L, Zwingman TA, Sunkin SM, Oh SW, Zariwala HA, Gu H, Ng LL, Palmiter RD, Hawrylycz MJ, Jones AR, Lein ES, Zeng H. A robust and high-throughput Cre reporting and characterization system for the whole mouse brain. Nat Neurosci. 2010; 13:133–140. [PubMed: 20023653]
48. Suzuki T, Arumugam P, Sakagami T, Lachmann N, Chalk C, Sallese A, Abe S, Trapnell C, Carey B, Moritz T, Malik P, Lutzko C, Wood RE, Trapnell BC. Pulmonary macrophage transplantation therapy. Nature. 2014; 514:450–454. [PubMed: 25274301]
49. Miksa M, Komura H, Wu R, Shah KG, Wang P. A novel method to determine the engulfment of apoptotic cells by macrophages using pHrodo succinimidyl ester. J Immunol Meth. 2009; 342:71–77.
50. Jakubzick C, Tacke F, Llodra J, van Rooijen N, Randolph GJ. Modulation of dendritic cell trafficking to and from the airways. J Immunol. 2006; 176:3578–3584. [PubMed: 16517726]
51. Westphalen K, Gusarova GA, Islam MN, Subramanian M, Cohen TS, Prince AS, Bhattacharya J. Sessile alveolar macrophages communicate with alveolar epithelium to modulate immunity. Nature. 2014; 506:503–506. [PubMed: 24463523]
52. Soderland SC, Naum Y. Letter: Growth of pulmonary alveolar macrophages in vitro. Nature. 1973; 245:150–152. [PubMed: 4582665]
53. Trapnell BC, Whitsett JA. Gm-CSF regulates pulmonary surfactant homeostasis and alveolar macrophage-mediated innate host defense. Ann Rev Physiol. 2002; 64:775–802. [PubMed: 11826288]

54. Kohyama M, Ise W, Edelson BT, Wilker PR, Hildner K, Mejia C, Frazier WA, Murphy TL, Murphy KM. Role for Spi-C in the development of red pulp macrophages and splenic iron homeostasis. Nature. 2009; 457:318–321. [PubMed: 19037245]
55. Haldar M, Kohyama M, So AY, Kc W, Wu X, Briseno CG, Satpathy AT, Kretzer NM, Arase H, Rajasekaran NS, Wang L, Egawa T, Igarashi K, Baltimore D, Murphy TL, Murphy KM. Heme-mediated SPI-C induction promotes monocyte differentiation into iron-recycling macrophages. Cell. 2014; 156:1223–1234. [PubMed: 24630724]
56. Rosas M, Davies LC, Giles PJ, Liao CT, Kharfan B, Stone TC, O'Donnell VB, Fraser DJ, Jones SA, Taylor PR. The transcription factor Gata6 links tissue macrophage phenotype and proliferative renewal. Science. 2014; 344:645–648. [PubMed: 24762537]
57. Gautier EL, Ivanov S, Williams JW, Huang SC, Marcelin G, Fairfax K, Wang PL, Francis JS, Leone P, Wilson DB, Artyomov MN, Pearce EJ, Randolph GJ. Gata6 regulates aspartoacylase expression in resident peritoneal macrophages and controls their survival. J Exp Med. 2014; 211:1525–1531. [PubMed: 25024137]
58. Okabe Y, Medzhitov R. Tissue-specific signals control reversible program of localization and functional polarization of macrophages. Cell. 2014; 157:832–844. [PubMed: 24792964]
59. Washino S, Ando H, Ushijima K, Hosohata K, Kumazaki M, Mato N, Sugiyama Y, Kobayashi Y, Fujimura A, Morita T. Temsirolimus induces surfactant lipid accumulation and lung inflammation in mice. Am J Physiol Lung Cell Mol Physiol. 2014; 306:L1117–1128. [PubMed: 24793166]
60. Salmond RJ, Emery J, Okkenhaug K, Zamoyska R. MAPK, phosphatidylinositol 3-kinase, and mammalian target of rapamycin pathways converge at the level of ribosomal protein S6 phosphorylation to control metabolic signaling in CD8 T cells. J Immunol. 2009; 183:7388–7397. [PubMed: 19917692]
61. Kim K, Qiang L, Hayden MS, Sparling DP, Purcell NH, Pajvani UB. mTORC1-independent Raptor prevents hepatic steatosis by stabilizing PHLPP2. Nat Commun. 2016; 7:10255. [PubMed: 26743335]
62. Gosselin D V, Link M, Romanoski CE, Fonseca GJ, Eichenfield DZ, Spann NJ, Stender JD, Chun HB, Garner H, Geissmann F, Glass CK. Environment drives selection and function of enhancers controlling tissue-specific macrophage identities. Cell. 2014; 159:1327–1340. [PubMed: 25480297]
63. Pham PTT, Pham PCT, Danovitch GM, Ross DJ, Gritsch HA, Kendrick EA, Singer J, Shah T, Wilkinson AH. Sirolimus-Associated Pulmonary Toxicity. Transplant. 2004; 77:1215–1220.
64. Weichhart T, Costantino G, Poglitsch M, Rosner M, Zeyda M, Stuhlmeier KM, Kolbe T, Stulnig TM, Horl WH, Hengstschlager M, Muller M, Saemann MD. The TSC-mTOR signaling pathway regulates the innate inflammatory response. Immunity. 2008; 29:565–577. [PubMed: 18848473]
65. Mitchell AJ, Pradel LC, Chasson L, Van Rooijen N, Grau GE, Hunt NH, Chimini G. Technical advance: autofluorescence as a tool for myeloid cell analysis. J Leuk Biol. 2010; 88:597–603.

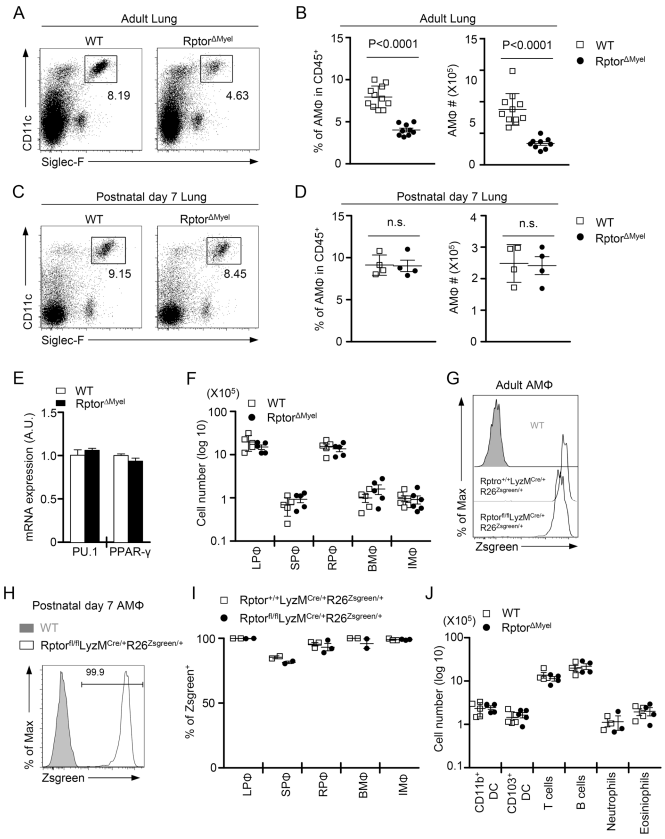

Figure 1. Loss of Raptor results in a reduction of AMΦ pool in adult mice

(A) Representative dot plots of $CD45^+$ living cells from single cell preparations of enzymatically digested lung from adult (6–9 weeks old) WT and $Rptor^{\Delta Myel}$ mice.

(B) Frequencies and absolute numbers of AMΦ from 6–16 weeks old WT and $Rptor^{\Delta Myel}$ mice. Each circle or square represents on mouse of the indicated genotypes. Data are expressed as mean ± SEM; n ≥ 9 per group.

(C) Representative dot plots of $CD45^+$ living cells from single cell preparations of enzymatically digested lung from WT and $Rptor^{\Delta Myel}$ mice at the age of 7 days.

(D) Frequencies and absolute numbers of AMΦ from WT and $Rptor^{\Delta Myel}$ mice at the age of postnatal day 7. Data are expressed as mean ± SEM; n ≥ 4 per group. n.s., non-significant.

(E) Quantitative real-time PCR analysis of *PU.1* and *PPAR-γ* mRNA in sorted AMΦ; results are presented relative to those of the control gene *β-actin*. Data are shown as mean ± SEM of triplicates and are representative of two independent experiments.

(F) Quantification of macrophages from various tissues, including interstitial macrophages (IMΦ) of the lung, large peritoneal macrophages (LPΦ), small peritoneal macrophages (SPΦ), spleen red pulp macrophages (RPΦ), and bone marrow macrophages (BMΦ). Data are expressed as mean ± SEM; n ≥ 5 per group.

(G – I) *Zsgreen* reporter expression was analyzed in macrophages with indicated genotypes. Representative histograms show *Zsgreen* levels in AMΦ from adult mice **(G)** and 7 days old mice **(H). (I)** $Zsgreen^+$ cells among macrophages from various tissues in adult mice. Data are expressed as mean ± SEM; n ≥ 2 per group.

(J) Indicated leucocytes counts in the lung from WT and Rptor$^{\Delta Myel}$ mice. Data are expressed as mean ± SEM; n ≥ 3 per group.

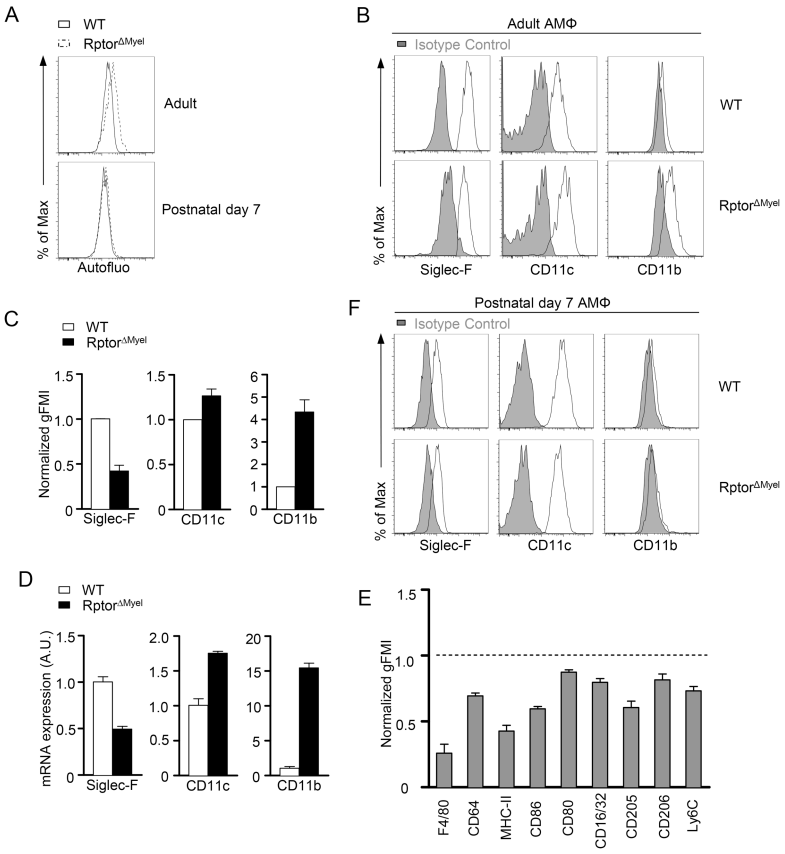

Figure 2. Raptor deletion altered AMΦ surface profile

(A) Autofluorescence(Autofluo) of unstained AMΦ from WT or Rptor$^{\Delta myel}$ adult and 7 days old mice measured at violet excited emission by flow cytometry.

(B and C) Siglec-F, CD11c and CD11b expression in WT and Rptor$^{\Delta Myel}$ AMΦ from adult mice. Overlaid histograms **(B)** with isotype control shown in solid gray. **(C)** Normalized geometric mean fluorescence intensity (gFMI). Results are presented relative to WT AMΦ (set as 1). Data are expressed as mean ± SEM; n ≥ 4 per group.

(D) Real-time qPCR analysis of Siglec-F, CD11c and CD11b mRNA levels in sorted AMΦ. Data are shown as mean ± SEM of triplicates and are representative of two independent experiments.

(E) Relative gMFI of various molecules in Rptor$^{\Delta Myel}$ AMΦ measured by flow cytometry. Results are presented relative to WT AMΦ (set as 1). Data are expressed as mean ± SEM; n ≥ 3 per group.

(F) Siglec-F, CD11c and CD11b expression in AMΦ from 7 days old WT and Rptor$^{\Delta Myel}$ mice. Isotype control is shown in solid gray.

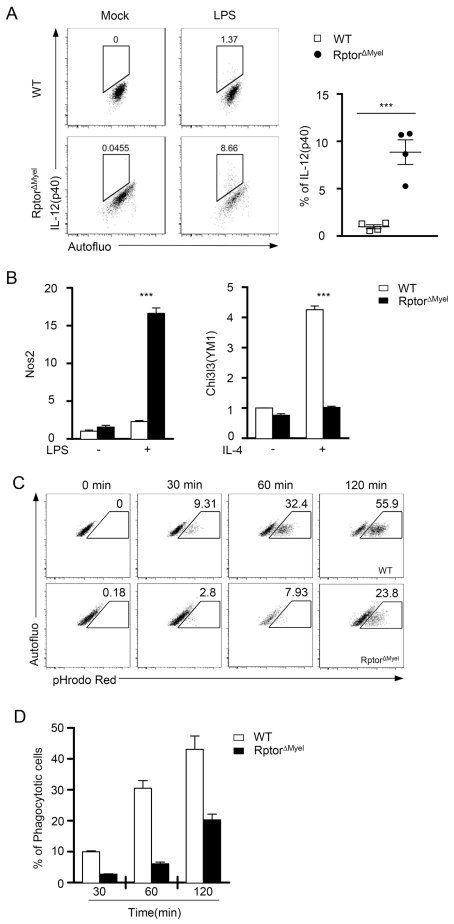

Figure 3. Raptor deficiency altered AMΦ M1/M2 polarization and phagocytosis function

(A,B) AMΦ were purified from freshly isolated bronchoalveolar lavage from WT and Rptor$^{\Delta myel}$ mice, followed by stimulation with LPS (10 ng/ml) or IL-4 (10 ng/ml), for 6 hours or 24 hours, respectively. (A) (Left) Intracellular flow cytometry analysis for IL-12 (p40) in AMΦ stimulated with LPS. (Right) Representative Data are expressed as mean ± SEM; n = 4 per group. (B) Quantitative real time PCR analysis for expression of (left) M1 hallmark gene *Nos2* or (right) M2 hallmark gene *Chi3l3*, alias *YM1*, upon stimulation by LPS or IL-4, respectively. Data are shown as mean ± SEM of triplicates and are representative of two independent experiments**. (C, D)** Impaired phagocytosis of apoptotic thymocytes by *Raptor* deficient AMΦ. WT and Rptor$^{\Delta Myel}$ AMΦ were incubated with apoptotic thymocytes pre-labeled with pHrodo for indicated time. **(C)** Representative dot-plots shown pHrodo Red intensity in gated AMΦ. Gating strategy for identification of AMΦ is shown in Supplementary Fig. S2B**. (D)** Bar-graphs showing mean ± SEM of pHrodo Red positive AMΦ. n ≥ 5 per group.

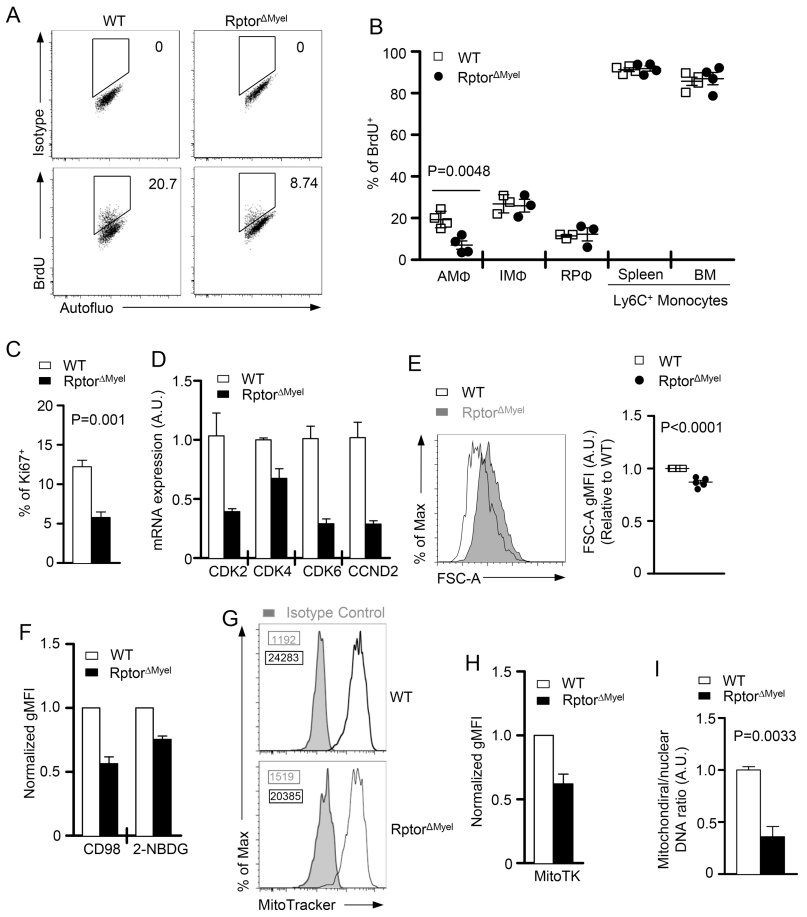

Figure 4. Essential role of mTORC1 for AMΦ proliferation in vivo

(A, B) WT and Rptor$^{\Delta Myel}$ mice were i.p. administered with 1.5mg BrdU per day for 7 consecutive days prior to flow cytometric analysis of cells in various tissues. Gating strategy to identify AMΦ is shown in Supplementary Fig. S3C**. (A)** Representative dot-plots depict the percentage of BrdU staining among AMΦ from WT and Rptor$^{\Delta Myel}$ mice. **(B)** **P**ercentage of BrdU^{+} cells among AMΦ, IMΦ, RPΦ, Ly6c^{+} monocytes in spleen and bone marrow. Data are expressed as mean ± SEM; n ≥ 3 per group.

(C) Percentages of Ki67^{+} AMΦ. Data are expressed as mean ± SEM; n ≥ 4 per group.

(D) *CDK2*, *CDK4*, *CDK6* and *CCND2* mRNA in sorted AMΦ measured by **r**eal-time qPCR. Data are shown as mean ± SEM of triplicates and are representative of two independent experiments.

(E) AMΦ cell sizes from WT and Rptor$^{\Delta Myel}$ adult mice indicated by forward side scatter (FSC). Representative overlaid histograms and relative gMFI of FSC are shown. Data are expressed as mean ± SEM; n ≥ 6 per group.

(F) Expression of CD98, 2-NBDG uptake, and MitoTracker staining of Rptor$^{\Delta Myel}$ AMΦ relative to WT AMΦ (set as 1). Data are expressed as mean ± SEM; n ≥ 4 per group.

(F) Representative overlaid histograms of MitoTracker staining of Rptor$^{\Delta Myel}$ AMΦ

(G) Bar graphs are mean ± SEM of the relative MitoTracker staining intensity of WT and Rptor$^{\Delta Myel}$ AMΦ. n = 3 per group.

(I) Mitochondrial DNA copies were measured by quantitative PCR, and normalized to nuclear DNA levels in a ratio of mitochondrial 12S rDNA over genomic 18S rDNA. Data are shown as mean ± SEM of triplicates and are representative of two independent experiments.

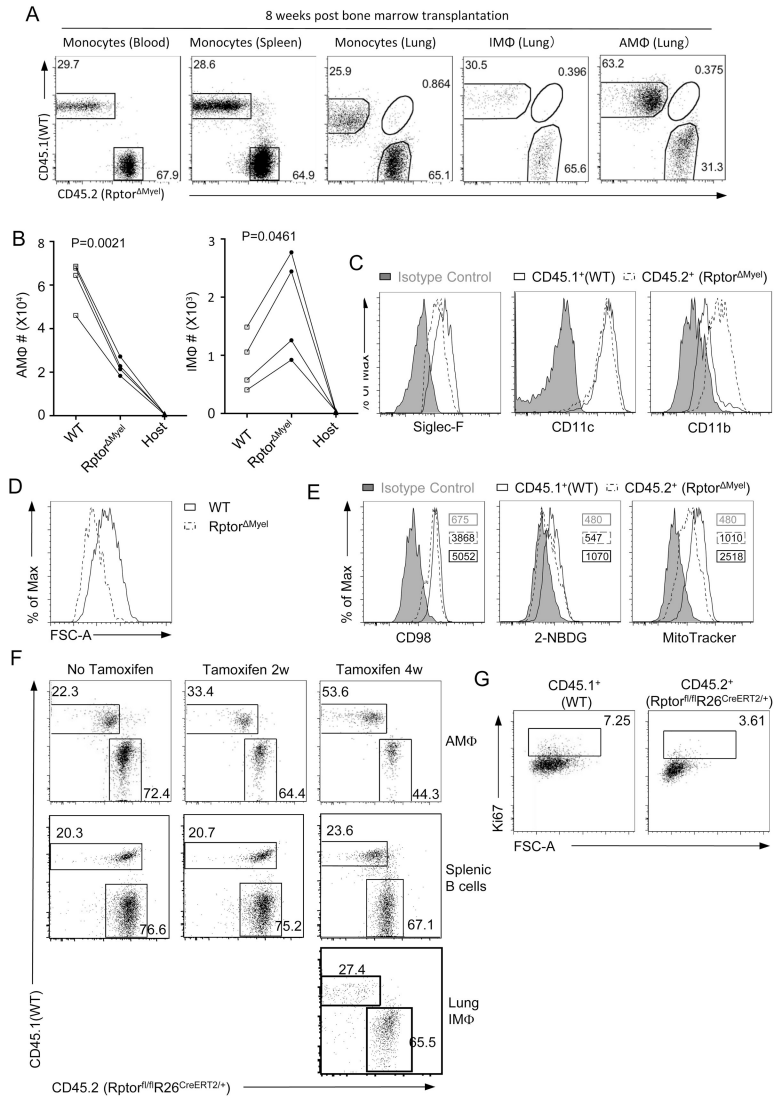

Figure 5. Raptor is required for AMΦ proliferation during irradiation-induced replenishment

(A – E) Lethally irradiated recipient mice ($CD45.1^+CD45.2^+$) were transplanted with mixed bone marrow cells from WT ($CD45.1^+$) and $Rptor^{\Delta myel}$ ($CD45.2^+$) donor mice. Chimeric mice were analyzed 8 weeks later. **(A)** Dot-plots show distribution of WT and $Rptor^{\Delta myel}$ blood, spleen, and lung monocytes and lung IMΦ and AMΦ. Monocytes obtained from peripheral blood and spleen were defined as $7AAD^-SSC^{low}CD45^+CD11b^+CD115^+Ly6G^-$, and that from lung were defined as $7AAD^-SSC^{low}CD45^+CD11b^+Autofluo^-Siglec\text{-}F^-F4/80^+$. IMΦ and AMΦ were gated as described in Fig. S1. **(B)** Donor-derived and host IMΦ and AMΦ numbers in chimeric mice. Connected lines represent individual chimeric mice. **(C)** Siglec-F, CD11c, CD11b expression, **(D)** FSC-A as measurement of cell size, and **(E)** CD98 expression, 2-NBDG uptake, and MitoTracker staining in donor-derived WT and $Rptor^{\Delta myel}$ AMΦ. Isotype control is shown in solid gray. Numbers in the plot indicated gMFI of relevant cells. Data shown are representative to two experiments.

(F, G) Bone marrow chimeric mice were generated by adoptive transfer mixed bone marrow cells from WT ($CD45.1^+$) and $Rptor^{fl/fl}R26^{CreERT2/+}$ ($CD45.2^+$) mice into lethally irradiated WT host mice ($CD45.1^+CD45.2^+$). 8 weeks after reconstitution, chimeric mice were i.p. administered with or without 2 mg tamoxifen for a total 4 times to "acutely" delete *Raptor*. **(F)** Donor-derived WT and Raptor deficient AMΦ and splenic $B220^+$ B cells in recipients without tamoxifen treatment and 2 weeks or 4 weeks after initial tamoxifen treatment or lung IMΦ 4 weeks after initial tamoxifen treatment. **(G)** Ki67 staining in donor derived WT and Raptor deficient AMΦ.

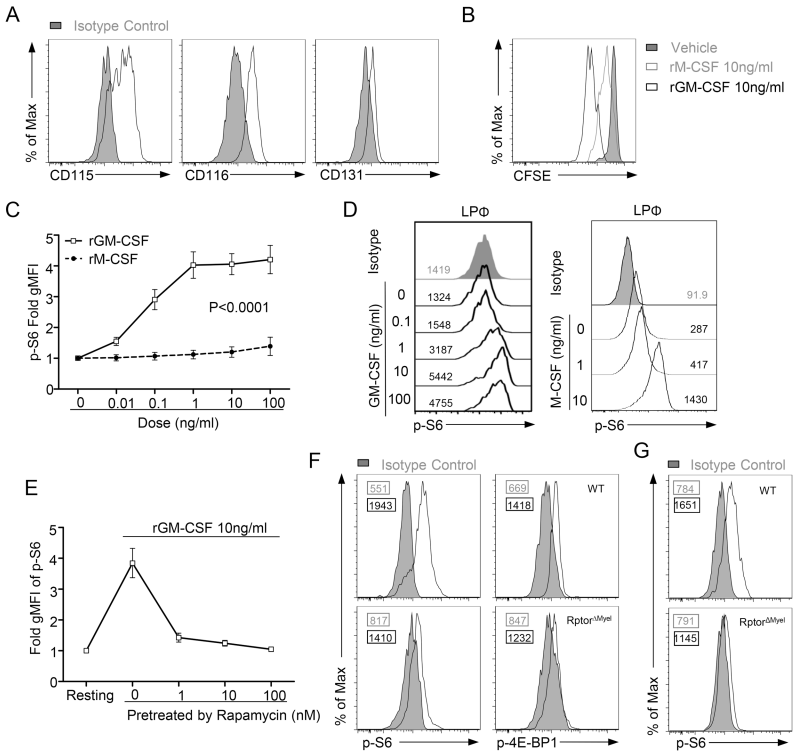

Figure 6. mTORC1 activation in AMΦ is induced upon GM-CSF stimulation

(A) CD115, CD116 and CD131 expression in WT AMΦ. Isotype control is shown in solid gray.

(B) CFSE (carboxyfluorescein succinimidyl ester) dilution in WT AMΦ cultured with rGM-CSF (10ng/ml), rM-CSF (10ng/ml), or vehicle for 5 days *in vitro*.

(C, D) Cells obtained by bronchoalveolar lavage or peritoneal capacity lavage from WT mice were *ex vivo* stimulated with varying doses of recombinant murine GM-CSF (rGM-CSF), recombinant murine M-CSF (rM-CSF), or vehicle (PBS) for 30 min. S6 phosphorylation (p-S6) on gated live macrophages were analyzed by flow cytometry. **(C)** Cumulative data of gMFI of p-S6 in AMΦ; results are presented relative to vehicle control (set as 1). Data are expressed as mean ± SEM; n ≥ 4 per group. **(D)** Representative histogram showing p-S6 in live LPΦ cultured with rM-CSF. Isotype control is shown in solid gray. Numbers in the plots indicated gMFI of relevant cells. *p* value was determined using a two-way ANOVA test.

(E) Inhibition of rGM-CSF-induced pS6 in AMΦ by rapamycin pretreatment. AMΦ were pretreated with rapamycin at the indicated concentrations followed by stimulation with 10ng/ml rGM-CSF for 30 min; results are presented relative to resting cells (set as 1). Data are expressed as mean ± SEM; n=3.

(F, G) Representative flow cytometry analysis of S6 or 4E-BP1 phosphorylation (p-4E-BP1) in fleshly isolated AMΦ from WT and Rptor$^{\Delta myel}$ adult mice **(F)** or 7 days old mice **(G)**. Numbers in the plot indicated gMFI of relevant cells.

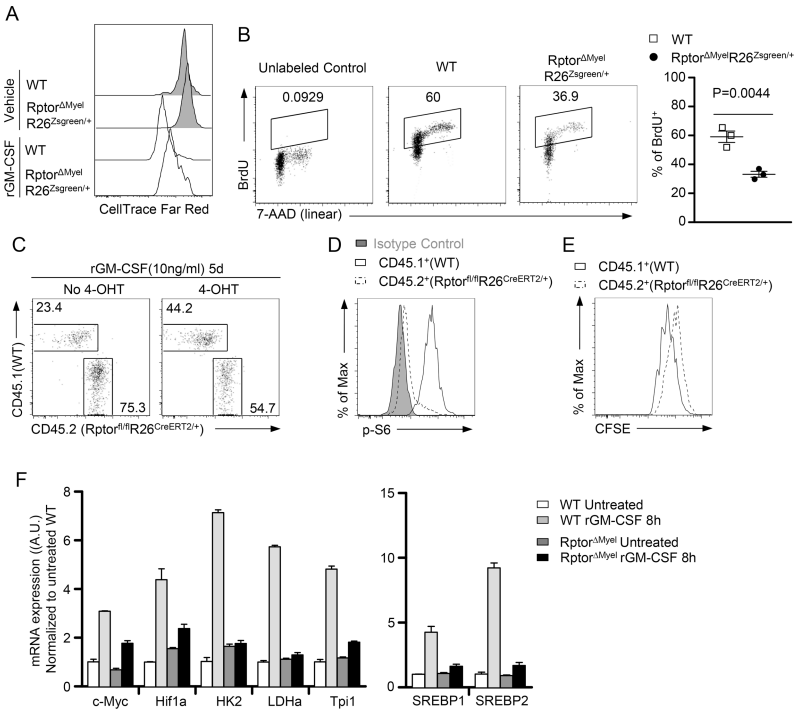

Figure 7. Raptor confers AMΦ optimal proliferative response to GM-CSF

(A, B) Equal numbers of WT (*Zsgreen* reporter negative) and Rptor$^{\Delta myel}$ R26$^{Zsgreen/+}$ (*Zsgreen* reporter positive) AMΦ were not labeled (B) or labeled with CellTrace Far Red (A) and co-cultured *in vitro* in the presence of 10 ng/ml rGM-CSF or vehicle for 5 days (**A**) or 80 hours with the addition of 10 μM BrdU in the last 8 hours (B). **(A)** Histograms show CellTrace Far Red dilution in WT (Zsgreen^{-}) and Rptor$^{\Delta myel}$ (ZsGreen^{+}) AMΦ. **(B)** BrdU and DNA content staining in WT (Zsgreen^{-}) and Rptor$^{\Delta myel}$ (ZsGreen^{+}) AMΦ. Scatter plot summarizes data of three independent experiments. Data are expressed as mean ± SEM.

(C – E) AMΦ chimeric mice (CD45.1^{+}CD45.2^{+}) reconstituted with a mixture of WT (CD45.1^{+}) and Rptor$^{fl/fl}$R26$^{CreERT2/+}$ (CD45.2^{+}) bone marrows as described in Figure 5F and 5G without tamoxifen treatment were cultured *in vitro* in the presence of 10 ng/ml rGM-CSF in the presence or absence of 0.5 μM 4-OHT for 5 d. (**C)** Representative dot-plots showing donor derived AMΦ.

(D) S6 phosphorylation in donor derived AMΦ treated with 4-OHT. **(E)** CFSE dilution of AMΦ initially labeled with CFSE and cultured with 4-OHT for 5d. Results are representative of two independent experiments.

(F) Sorted AMΦ from WT or Rptor$^{\Delta myel}$ were cultured in vitro in the presence of rGM-CSF 10ng/ml for 8h, followed by real-time qPCR of indicated genes. Fleshly sorted cells served as untreated control. Data are expressed as mean ± SEM.